Microstructure and mechanical properties of mechanically alloyed ODS copper alloy for fusion material application

S. M. S. Aghamiri[*,1], N. Oono[1], S. Ukai[1], R. Kasada[2], H. Noto[3], Y. Hishinuma[3], T. Muroga[3]

[1]*Graduate School of Engineering, Hokkaido University, Sappor 060-8628, Japan*

[2] *Institute of Advanced Energy, Kyoto University, Kyoto 611-0011, Japan*

[3]*National Institute of Fusion Science, Gifu 509-5202, Japan*

Abstract

Advanced oxide dispersion strengthened copper alloys are promising structural materials for application in divertor system of future fusion reactors due to high irradiation resistance, high thermal conductivity, and good mechanical properties. In this study, a new ODS copper including 0.42wt%Y_2O_3 nanosized oxide particles was developed successfully by mechanical alloying method using addition of 1wt% Stearic acid in Ar atmosphere. Mechanical alloying resulted in decrease of crystallite size to 28nm in concurrent with increment of dislocation density and hardness to the saturated level of $1.7 \times 10^{15} m^{-2}$ and 226$HV_{0.1}$ after 48hours milling, respectively. Consolidated ODS copper by SPS and then hot roll-annealing at 900ºC/60min showed an average grain size of 1.1 μm with a near random texture. Furthermore, TEM observations demonstrated fine semicoherent Y_2O_3 oxide particles distributed with a misfit parameter (δ) of 0.17 in copper matrix with an average size of 10.8nm and interparticle spacing of 152nm. Finally, tensile test evaluation determined comparable mechanical properties of the annealed ODS copper (Cu-0.42wt%Y_2O_3) with Glidcop-Al25 including a yield strength of 272MPa and total elongation of 12%, by two mechanisms of grain boundary strengthening and oxide particle strengthening.

Keywords: ODS copper, Mechanical alloying; Microstructure, Mechanical properties

1. Introduction

* Corresponding author. Hokkaido University, Sappor 060-8628, Japan.

Email Address: sms.aghamiri@gmail.com

Advanced copper alloys are the main candidate for high heat flux and high temperature materials application in different components of fusion energy reactors such as divertor due to extremely high energy density. Key properties of high thermal conductivity (~300-400 W/m.K), good mechanical property (yield strength >200 MPa) and high irradiation resistance (especially irradiated-condition ductility) are essential for effective performance of these materials in a high heat flux, high irradiation environment [1].

Up to now, two main category of copper alloy have been developed for fusion application: Precipitation strengthened (PS) copper alloys and Dispersion strengthened (DS) copper alloys [1-4]. PS copper alloys such as CuCrZr (used in ITER reactor) or CuNiBe can be strengthened considerably by fine precipitation of second phase particles. The main problem of PS copper alloys is softening by coarsening of precipitates at intermediate to high temperatures. DS copper alloys have the benefit of keeping the strength even at elevated temperatures by dispersion of fine stable oxide particles. The main commercially available dispersion-strengthened copper alloys are Glidcop-Al15, Al25, Al60 and MAGT 0.2, all produced by internal oxidation method. These alloys are strengthened by dispersion of fine alumina particles inside the copper matrix during their manufacturing process. However, both developed copper alloys have the serious limitation of low ductility after irradiation [5,6].

Oxide dispersion strengthened (ODS) alloys are the attractive option for the irradiation environments because of good mechanical properties and irradiation resistance. It has been proved that dispersion of fine Y_2O_3 oxide particles in ODS Steels have an important role to keep the mechanical properties and good irradiation resistance by capturing of defects and reducing irradiation swelling [7,8]. Up to now, the best developed way for good dispersion of Y_2O_3-based oxide particles in different ODS materials is mechanical alloying (MA) [8,9]. However, there is only few studies in literature regarding mechanical alloyed (MAed) ODS copper alloys with a limited progress [10-13]. It is expected to promote the mechanical properties by appropriate dispersion of fine oxide particles in a well-designed copper matrix. To develop new ODS copper with superior properties by MA method, at first, it needs to overcome the severe sticking of milled powder induced by high ductility of copper. Cryo-ball milling by liquid nitrogen has been reported to be used as successful milling method for dispersion of nanosized yttria and calcia in copper alloy [14,15]. In this study, a room temperature milling was studied in an alloy with a nominal composition of Cu-0.5wt% Y_2O_3 by addition of processing control agent (1wt% stearic acid (SA)) during milling in Ar atmosphere. After consolidation followed by hot rolling and subsequent annealing at 900°C, the mechanical properties of the ODS copper alloy were evaluated based on microstructural characterization.

2. Experimental

In this research, a high purity (99.9%) copper powder (particle size of ~50 μm) and Y_2O_3 nanopowder (particle size of ~50 nm) were used as raw materials. The powder mixture was mechanically alloyed by using Fritch-P6 planetary ball mill with different additions of stearic acid up to 2wt % as process control agent (PCA) in Ar atmosphere. 1wt% stearic acid was chosen as the optimum amount based on the higher powder output and purity of MA powder. The ball milling was performed with ball to powder ratio of 10:1 and rotation speed of 470 rpm in different milling times up to 96 hours. After the milling, the chemical composition of the powder was analyzed by inductively coupled plasma (ICP) method.

X-ray diffraction was conducted by means of $Cu-K\alpha$ radiation with a Philips X´Pert PRO to characterize the phases during milling. The change in crystallite size (D) during MA can be calculated from XRD broadening based on the Hall–Williamson equation [16]:

$$\beta_s \cos\theta = 2\,\varepsilon\, sin\ \theta + (K\lambda\ /D) \qquad (1)$$

where β_s is the peak full width at the half maximum intensity (FWHM) (after subtracting the instrumental broadening), θ is the diffraction angle, ε is the local strain, λ is the X-ray wavelength of the Cu-Kα (0.154 nm) and K is the Scherrer constant (0.9), respectively. Moreover, the dislocation density (ρ) can be correlated in terms of local strain (ε) in the following equation [16]:

$$\rho = 7.14\left(\frac{\varepsilon}{b}\right)^2 \qquad (2)$$

where b is Burger's vector (2.52×10^{-10}m). By measuring θ and β_s for the planes of (111), (200), (220), (311) and (222), the crystallite size (D) and dislocation density (ρ) were calculated and plotted versus milling time. This plot was accompanied with the average Vickers microhardness data of the milled powders measured by a HMV-Micro Hardness Tester-SHIMADZU, under a load of 980 mN by a diamond pyramid indenter and dwell time of 30 s with 10 times repetition. Vickers microhardness measurements were performed on each milled powder in different milling times after mounting the powder into the epoxy resin and polishing the surface.

The MAed ODS copper powder after 48 hours milling was consolidated by spark plasma sintering (SPS) at 900ºC/45min. Then the material was hot rolled at 900ºC with a 50% thickness reduction and a reduction rate of 0.5 mm per pass followed by annealing at

900ºC/60 min. The powder and bulk samples of ODS copper were observed by FESEM (JEOL JSM-6500F) equipped by Electron Back Scatter Diffraction (EBSD) detector. To attain Inverse Pole Figure (IPF) and Orientation distribution function (ODF), the EBSD data were analyzed by OIM software. The Sample preparation for EBSD was done by grinding with SiC paper up to 2000 grit and then polishing with 1 μm diamond paste and final polishing with silica suspension. A JEOL JEM-2010 transmission electron microscopy was used to study the oxide particles in the microstructure in high magnification with a voltage of 200 kV. Furthermore, a FEI-Titan STEM (300 kV) equipped with high-angle annular dark field (HAADF) detector and EDS analysis was used to analyze elemental distribution of fine oxide particles. The thin samples for TEM observation were prepared by focused ion beam (FIB) (JEOL JIB-4600F). For evaluation of oxide particle distribution, the interparticle spacing (λ) was derived from the below equations based on TEM images [9]:

$$\lambda = 1.25 l_s - 2r_s \quad (3)$$

$$l_s = \sqrt{\frac{2\pi\overline{r^3}}{3f\bar{r}}} \quad (4)$$

$$r_s = \frac{\pi\overline{r^2}}{4\bar{r}} \quad (5)$$

where, r is the particle radius obtained from the TEM images. $\bar{r}$ is the average oxide particle radius, and $\overline{r^2}$ and $\overline{r^3}$ are the averages of r^2 and r^3, respectively. The volume fraction of the dispersed oxide particles was estimated to be 0.0075 and the average distance between the centers of oxide particles is l_s. The average particle size is considered as D $(2r_s)$.

In order to evaluate mechanical properties, tensile test was performed at room temperature under a strain rate of 1.0×10^{-10}/S using Shimadzu, SSL-1KN tensile machine. Miniaturized size specimens for the tensile test were prepared with a gauge dimension of 5 mm in length, 1.2 mm in width and 0.5 mm in thickness by using an electro-discharge processing machine.

3. Results and discussions

3-1. Microstructure of ODS copper powder processed by MA in Ar Atmosphere

Fig. 1 shows the x-ray analyses of Cu-0.5wt%Y_2O_3 powder between 0 to 96 hours milling times in Ar atmosphere. In these curves, in addition to peaks of copper matrix, the

peaks of carbon compounds related to released PCA (Stearic acid) and yttrium oxide can be observed (as shown in the insets by arrows). However, yttrium oxide peak is hard to distinguish after 24 hours milling due to probable decomposition during high energy milling as discussed in different ODS materials [8]. Another point in this figure is broadening of copper peaks with increasing milling time which is the characteristic behavior of high strain mechanically milled powders caused by repeated cold welding, fracturing and rewelding of powder particles during milling [17].

Fig. 2(a) shows the evolution of crystallite size and dislocation density during increasing milling time calculated by equations (1) and (2). The curve demonstrates that crystallite size of powder particles decreases sharply in a short time and reach to the stable size of ~28 nm after about 48 hours. In other hand, trend of dislocation density shows a concurrent increase with decreasing crystallite size during milling time and saturates in the level of $1.7 \times 10^{15} m^{-2}$ after 48 hours. Change of Vickers microhardness of milled powders at different milling times in Fig. 2(b) determined consistent result with Fig.1, i.e. increasing the hardness and reaching to 226$HV_{0.1}$ after steady state condition of 48 hours milling.

Fig. 3 illustrates the ODS copper powder after mechanical alloying for 48 hours in Ar atmosphere. As shown in this figure, a fine and loose powder with irregular-shaped particles of ~100 μm average size was obtained after the high energy milling. The milling conditions resulted in a high powder recovery of 94% without agglomeration and sticking of ductile copper powder to milling cup by using optimum amount of 1wt% stearic acid which balanced the rate of cold welding and fracturing of powder particles [17]. The chemical composition of the mechanical alloyed ODS copper powder has been specified in Table 1. This composition indicates a copper alloy containing 0.42wt% Y_2O_3 oxide particles which suggests dissipation of some oxide powder during evacuation of MA pot atmosphere to replace with Ar. In addition, some minor impurity of iron, Ex. O and carbon were inserted from milling medium, atmosphere and releasing of PCA during high energy milling, respectively. The solute iron can decrease the thermal conductivity and segregation of carbon and Ex. O has been reported to result in intermediate temperature embrittlement [1,13]. So, to reach a sample with higher purity and hence higher thermal conductivity, some modifications in MA and thermal treatment in hydrogen environment [17] need to be done.

3-2. Microstructure of consolidated MAed ODS copper alloy by SPS and then hot roll-annealing

Fig. 4 shows the EBSD results of 48 hours-MAed ODS copper alloy consolidated by

SPS and then hot rolling and subsequent annealing at 900ºC/60 min. The IPF map (Fig. 4(a)) shows a fine-grained microstructure with the average grain size of about 1.14 μm including some larger grains up to ~5 μm resulted from abnormal grain growth probably due to lower pinning force induced by low density of oxide particles. Formation of such a fine grain after sintering is the result of severe plastic deformation during MA which has been observed in different MA-processed ODS alloys [8-10]. Evaluation of grains orientations by ODF map at $\varphi_2 = 0°$ (Fig. 4(b)) represents a near random orientation of grains with a weak texture oriented in {110} plane including α-fiber of Goss orientation ({011} <100>) and near to Brass orientation ({011} <211>) and the other Cube orientation ({001} <100>) with a max. intensity of 2.05 times than random. Previous studies [18] on copper show that formation of α-fiber texture is a characteristic texture of some deformed copper alloys and cube orientation usually originates from the recrystallized copper grains. Therefore, this microstructure can be result of deformed-recrystallized condition during MA and subsequent hot roll-annealing.

Fig. 5(a-e) shows the HAADF-STEM image of consolidated ODS copper alloy with corresponding EDS map of existing elements as presented in Table 1. It can be observed many dark oxide particles distributed in the copper matrix enriched in the elements of Y and O, which confirms Y_2O_3 particles have dispersed in the matrix. In addition, while Fe shows a homogenous distribution in solution with copper, carbon segregated as fine particles beside the oxide particles or around the porosities at right-top of the images.

Fig. 6(a) illustrates TEM micrograph of consolidated ODS copper alloy suggesting fine Y_2O_3 nanoparticles were distributed homogenously both inside the grains and grain boundaries. Size distribution of the oxide particles in Fig. 6(b) shows that the oxide particles have a very small size up to 30 nm with an average size (D) of 10.8 nm and interparticle spacing (λ) of 152 nm. Misfit parameter (δ) between interface of oxide particles and copper matrix was calculated by the below equation [19]:

$$\delta = 2\frac{(d_1 - d_2)}{d_1 + d_2} \qquad (6)$$

where d_1 and d_2 are interplanar spacing of $(220)_{Cu}$ and $(444)_{Y_2O_3}$ planes with the values of 0.1328 nm and 0.1582 nm, respectively, measured from diffraction pattern in Fig. 6(c). The misfit parameter was calculated to be 0.17 between 0.25 (incoherent particles) and 0.05 (coherent particles). This misfit value indicates a semicoherent interface forms between oxide particles and copper matrix. Analysis of oxide particles according to Ashby-brown contrast [20] shown in Fig. 7 specified that finer oxide particles with the size of 5-15nm (constituting approximately 85% of total oxide particles

based on Fig. 6(b)) have a semicoherent interface (Fig. 7(a)) revealed by moire fringes. The larger oxide particles (remaining ~15% of total oxide particles) with the size of more than 15nm have an incoherent interface (Fig. 7(b)) with copper matrix.

3-3. Mechanical properties of hot rolled-annealed ODS Copper

The engineering stress-strain curve of 48 hours-MAed ODS copper alloy (Cu-0.42%wtY_2O_3) after SPS- hot rolling and subsequent annealing at 900ºC/60 min has been shown in Fig.8. It can be observed that this developed alloy has a 0.2% yield strength (σ_y) of 272 MPa with a total elongation (El.) of 12%. Comparing this result with pure copper (σ_y:65MPa, El.:45%) [1] shows an improvement of the strength in expense of lower elongation. This level of strength is comparable with Al oxide-dispersed Glidcop-Al25 alloy processed by internal oxidation method with mechanical properties of (σy:296MPa, El.:19%) [21].

To understand the strengthening mechanisms involved in this new developed ODS copper, it requires to calculate the contributed mechanisms as follow:

3-1) Grain boundary strengthening

To calculate the grain boundary effect on strengthening, it was used the Hall-Petch relation as below equation:

$$\sigma_{HP} = \sigma_0 + K_{HP} d^{-1/2} \quad (7)$$

where σ_0 is Peierls stress (which is near zero for copper [14]), K_{HP} as Hall–Petch constant (4.5 MPa. $mm^{1/2}$[14]), d as grain diameter (1.14 μm based on the IPF map in Fig. 4b). Based on these values, grain boundary strengthening (σ_{HP}) is calculated to be 133MPa.

3-2) Oxide particle strengthening

By using Orowan mechanism, the effect of oxide dispersion strengthening based on bypass of oxide particles by dislocation loop was calculated by the following relation:

$$\sigma_{Or} = 0.84 \frac{MGb}{2\pi r\sqrt{1-v}(\sqrt{3\pi/2f}-\pi/4)} \ln(\frac{\pi r}{4b}) \quad (8)$$

where M is Taylor factor (3.1), G is shear modulus (45.5 GPa), b is burgers vector (0.255nm) and v is Poisson′s ratio (0.34) [19], r and f are average radius and fraction of oxide particles, respectively (5.4 nm and 0.0075 based on TEM studies in the section 3-2). The contributed oxide particle strengthening in the ODS copper alloy is calculated to be 127MPa.

Sum of both grain boundary strengthening (133MPa) and oxide particle strengthening (127MPa) result in the total strength (σ_t) of 260MPa which is comparable to the experimental yield strength of 272MPa. The strengthening mechanisms discussed in this study are in consistent with prior work by Kudashov et al. [10]. The results suggest the control of microstructure to reach a finer grained microstructure in addition to higher density of oxide particles are the most effective ways to promote the mechanical properties.

4. Conclusions

In this study, a new ODS copper with a composition of Cu-0.42%wt Y_2O_3 was processed successfully by several processing steps: 1) MA using addition of 1wt% stearic acid in Ar atmosphere, 2) then consolidation by Spark plasma sintering and subsequent hot rolling at 900 ºC with 50% reduction and final annealing at 900ºC/60min. MA of powder after 48hour milling showed a high decrease of crystallite size to 28nm and increase of dislocation density and consequent Vickers microhardness to a high level of $1.7 \times 10^{15} m^{-2}$ and 226$HV_{0.1}$, respectively. At this milling time, a fine and loose MA powder was obtained with some minor elements of C, Ex. O and Fe. The microstructure of hot roll-annealed ODS copper showed an average grain size of 1.14 μm containing fine semicoherent Y_2O_3 oxide particles distributed in copper matrix with average grain size of 10.8nm and interparticle spacing of 152 nm. Based on two contributed mechanisms of grain boundary strengthening and oxide dispersion strengthening, the mechanical properties promoted to a yield strength of 272 MPa and elongation of 12% which shows a comparable result with the Glidcop-Al25 alloy and considerable increase of strength in comparison to pure copper.

Acknowledgment

This work is supported by Grant-in-Aid for Scientific Research(A), 16H02443, Japan Society for the Promotion of Science (JSPS).

Ref.

1. M. Li, S. J. Zinkle, Physical and Mechanical Properties of Copper and Copper Alloys, in: R.M.J. Konings (Eds.), Comprehensive Nuclear Materials, Vol. 4, Elsevier Ltd., 2012, pp. 667-690.
2. A.S. Pokrovsky, S.A. Fabritsiev, D.J. Edwards, S.J. Zinkle, A.F. Rowcli, Effect of neutron dose and irradiation temperature on the mechanical properties and structure of dispersion strengthened copper alloys, J. Nucl. Mater. 283-287 (2000) 404-408.

3. V.R. Barabash, G.M. Kalinin, S.A. Fabritsiev, S.J. Zinkle, Specification of CuCrZr alloy properties after various thermo-mechanical treatments and design allowables including neutron irradiation effects, J. Nucl. Mater. 417 (2011) 904–907.

4. S.J. Zinkle, Evaluation of high strength, high conductivity CuNiBe alloys for fusion energy applications, J. Nucl. Mater. 449 (2014) 277–289.

5. S.A. Fabritsiev, S.J. Zinkle, B.N. Singh, Evaluation of copper alloys for fusion reactor divertor and first wall components, J. Nucl. Mater. 233-237 (1996) 127- 137.

6. S.A. Fabritsiev, A.S. Pokrovsky, S.J. Zinkle, D.J. Edwards, Low-temperature radiation embrittlement of copper alloys, J. Nucl. Mater. 233-237 (1996) 513-518.

7. M. S. El-Genk, J. Tournier, A review of refractory metal alloys and mechanically alloyed-oxide dispersion strengthened steels for space nuclear power systems, J. Nucl. Mater. 340 (2005) 93–112.

8. S. Ukai, Oxide Dispersion Strengthened Steels, in: R.M.J. Konings (Eds.), Comprehensive Nuclear Materials, Vol. 4, Elsevier Ltd., 2012, pp. 241–271.

9. S.M. S. Aghamiri, H.R. Shahverdi, S. Ukai, N. Oono, K. Taya, S. Miura, S. Hayashi, T. Okuda, Microstructural characterization of a new mechanically alloyed Ni-base ODS superalloy powder, Mater. Charact. 100 (2015) 135–142.

10. D.V. Kudashov, H. Baum, U. Martin, M. Heilmaier, H. Oettel, Microstructure and room temperature hardening of ultra-fine-grained oxide-dispersion strengthened copper prepared by cryomilling, Mater. Sci. Eng. A 387–389 (2004) 768–771.

11. J. Groza, Heat-Resistant dispersion-strengthened copper alloys, J. Mater. Eng. Perf., Vol. 1, 113-121.

12. G. Carro a, A. Muñoz, M.A. Monge, B. Savoini, R. Pareja, C. Ballesteros, P. Adev, Fabrication and characterization of Y_2O_3 dispersion strengthened copper alloys, J. Nucl. Mater. 455 (2014) 655–659.

13. G. Carro, A. Munoz, M.A. Monge, B. Savoini, R. Pareja, Microstructural and mechanical characterization of Cu-0.8 wt.%Y, Fusion Eng. Des. 98–99 (2015) 1941–1944.

14. D.V. Kudashov, H. Baum, U. Martin, M. Heilmaier, H. Oettel, Microstructure and room temperature hardening of ultra-fine-grained oxide-dispersion strengthened copper prepared by cryomilling, Mater. Sci. Eng. A 387–389 (2004) 768–771.

15. U. Martin, M. Heilmaier, Novel DS metals by Mechanical Alloying, Adv. Eng. Mater. 7 (2004), 515-520.

16. L. Zhang, S. Ukai, T. Hoshino, S. Hayashi, X. Qu, Y_2O_3 evolution and dispersion refinement in Co-base ODS alloys, Acta Mater. 57 (2009) 3671–3682.

17. C. Suryanarayana, Mechanical alloying and milling, Prog. in Mater. Sci. 46 (2001) 1-184.

18. F.J. Humphreys and M. Hatherly, Recrystallization and related annealing phenomena, 2nd edition, Elsevier, 2004.

19. H. Zhuo, J. Tang, N. Ye, A novel approach for strengthening Cu–Y_2O_3 composites by in situ reaction at liquidus temperature, Mater. Sci. Eng. A 584 (2013) 1–6.

20. P. Dou, A. Kimura, T. Okuda, M. Inoue, S. Ukai, S. Ohnuki, T. Fujisawa, F. Abe, Polymorphic and coherency transition of Y–Al complex oxide particles with extrusion temperature in an Al-alloyed high-Cr oxide dispersion strengthened ferritic steel, Acta Mater. 59 (2011) 992–1002.

21. GLIDCOP® Dispersion Strengthened Copper datasheet, Hoganas High Alloys LLC, 2013. www.hoganas.com.

List of Figures

List of Tables

Table 1.

Specimen	Fe	Ex. O[a]	C	Y_2O_3[b]	Cu
MA ODS copper powder	**0.15**	**0.22**	**0.72**	**0.42**	**Balance**

[a]

E [a] Estimated from total oxygen content minus oxygen coupled with Y_2O_3 (wt% total oxygen – wt% Y×0.27).

[b] Estimated from Y content with assumption that Y exists as Y_2O_3 (1.27×wt% Y).

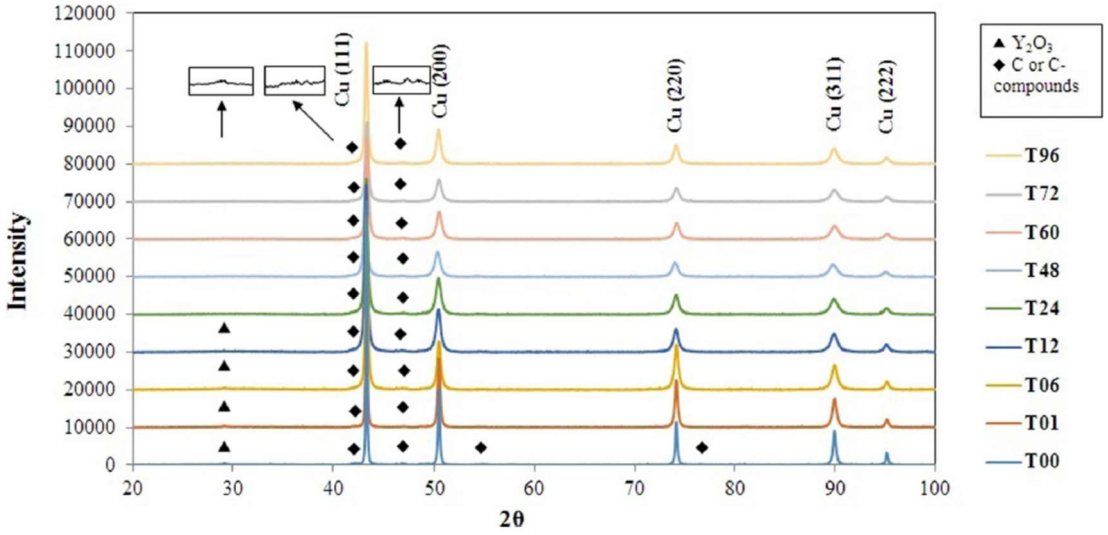
Intensity
2θ
Cu (111)
Cu (200)
Cu (220)
Cu (311)
Cu (222)
▲ Y_2O_3
◆ C or C-compounds
T96
T72
T60
T48
T24
T12
T06
T01
T00

Fig. 1

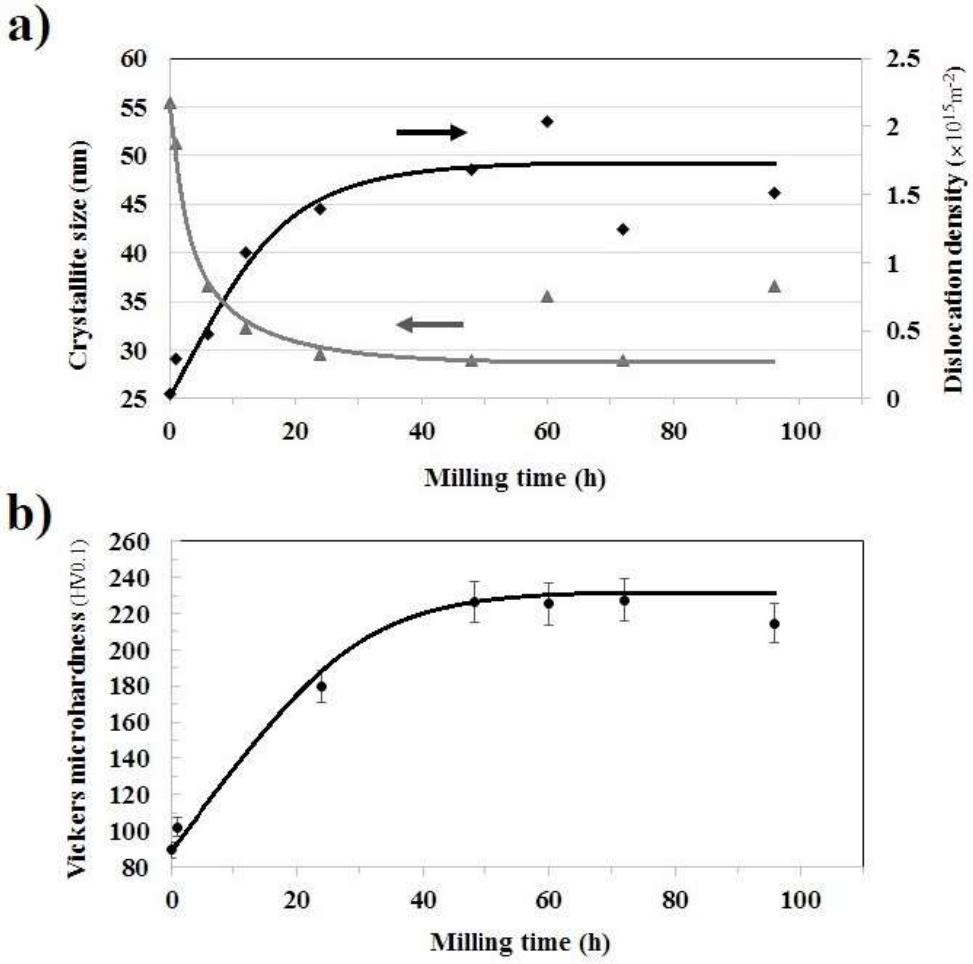
a)
Crystallite size (nm)
Dislocation density (×10^15 m^-2)
Milling time (h)
b)
Vickers microhardness (HV0.1)
Milling time (h)

Fig. 2

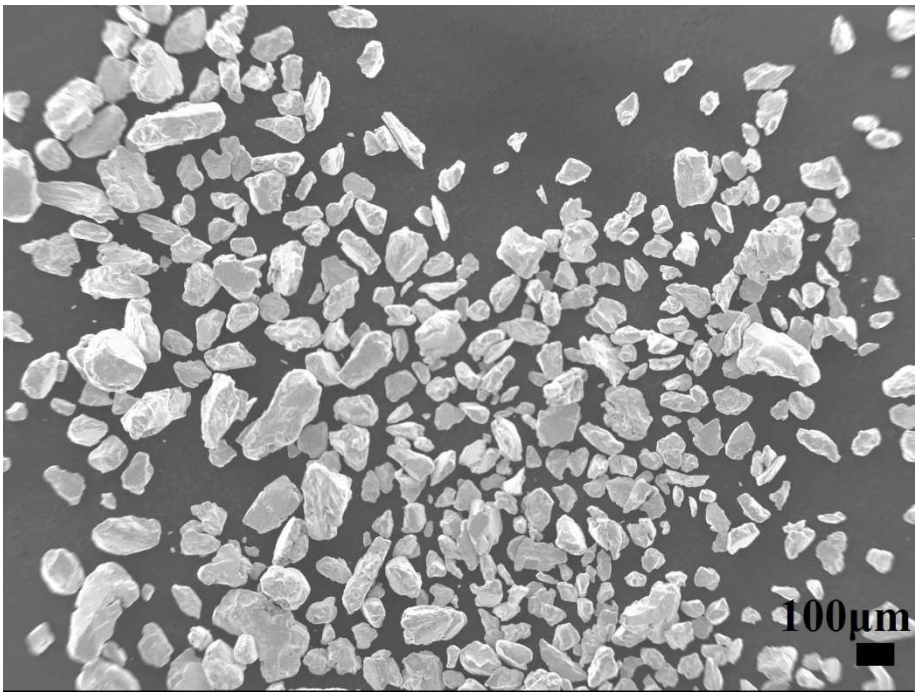
100µm

Fig. 3

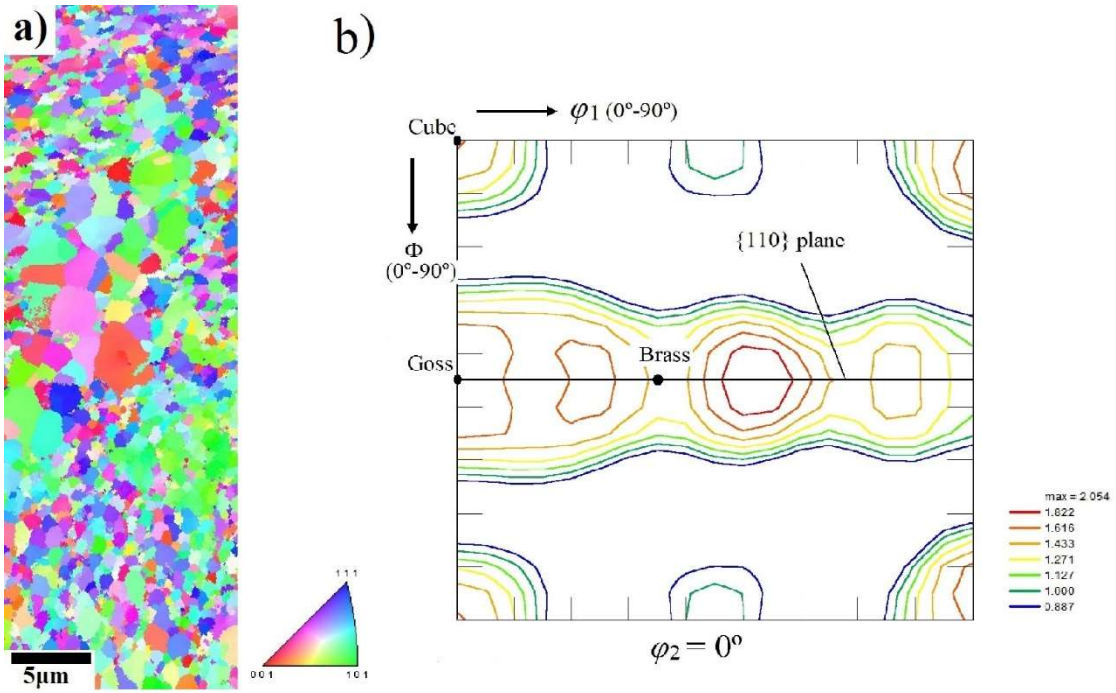
a)
5µm
111
001
101
b)
Cube
φ1 (0°-90°)
Φ
(0°-90°)
{110} plane
Goss
Brass
φ2 = 0°
max = 2.054
1.822
1.616
1.433
1.271
1.127
1.000
0.887

Fig. 4

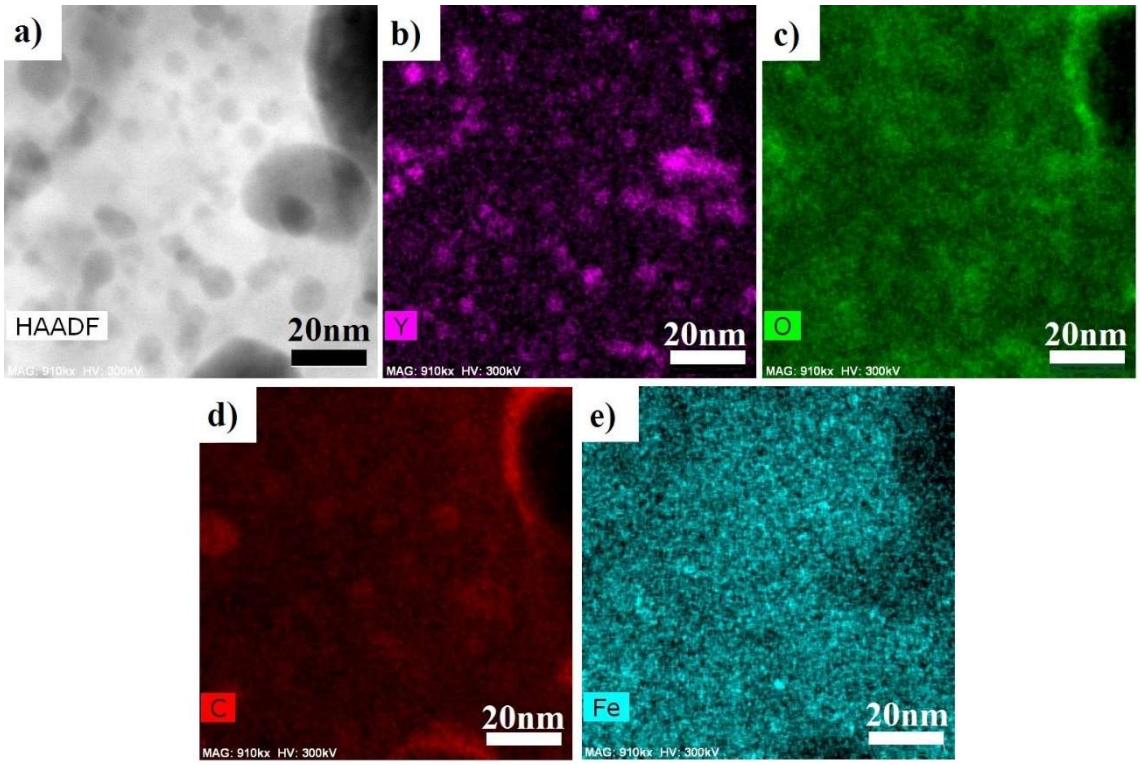
a)
HAADF
20nm
b)
Y
20nm
MAG: 910kx HV: 300kV
c)
O
20nm
MAG: 910kx HV: 300kV
d)
C
20nm
MAG: 910kx HV: 300kV
e)
Fe
20nm
MAG: 910kx HV: 300kV

Fig. 5

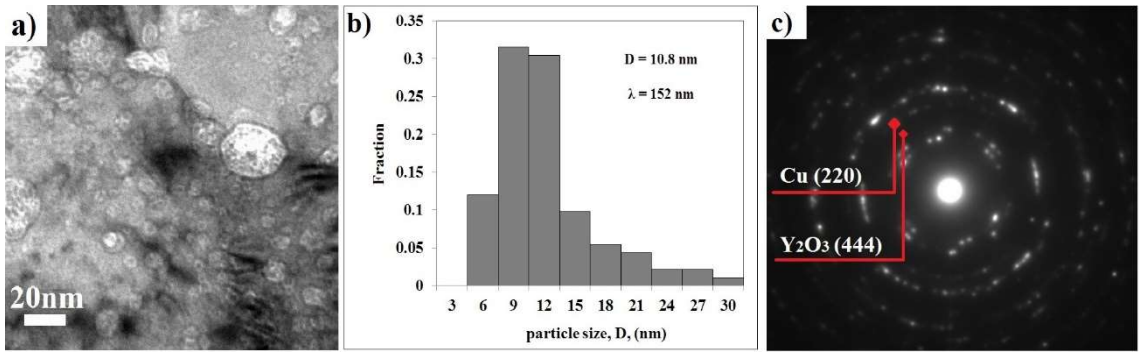
a)
20nm
b)
D = 10.8 nm
λ = 152 nm
Fraction
0.35
0.3
0.25
0.2
0.15
0.1
0.05
0
3 6 9 12 15 18 21 24 27 30
particle size, D, (nm)
c)
Cu (220)
Y2O3 (444)

Fig. 6

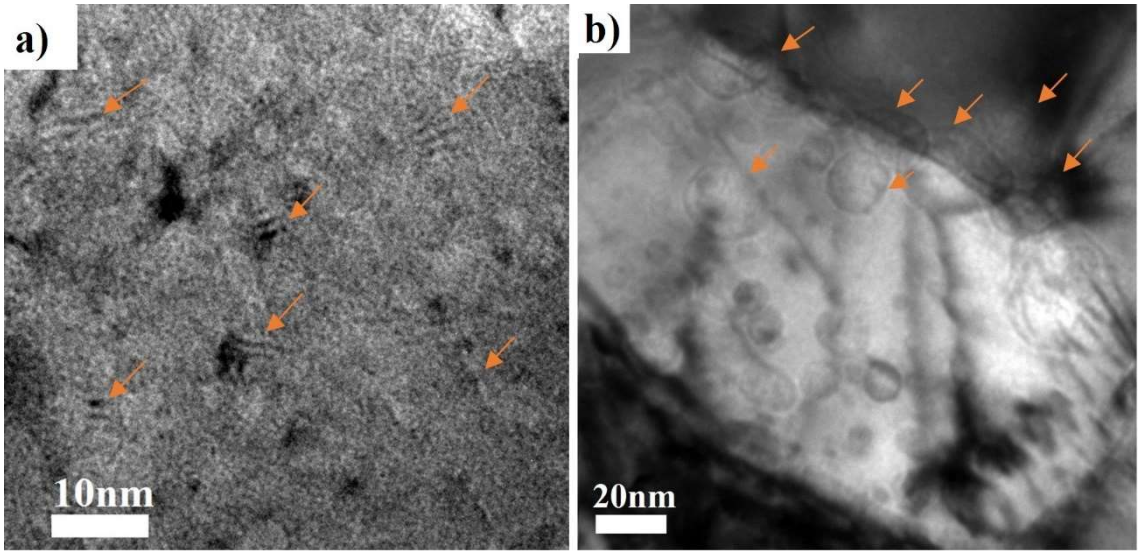
a)
10nm
b)
20nm

Fig. 7

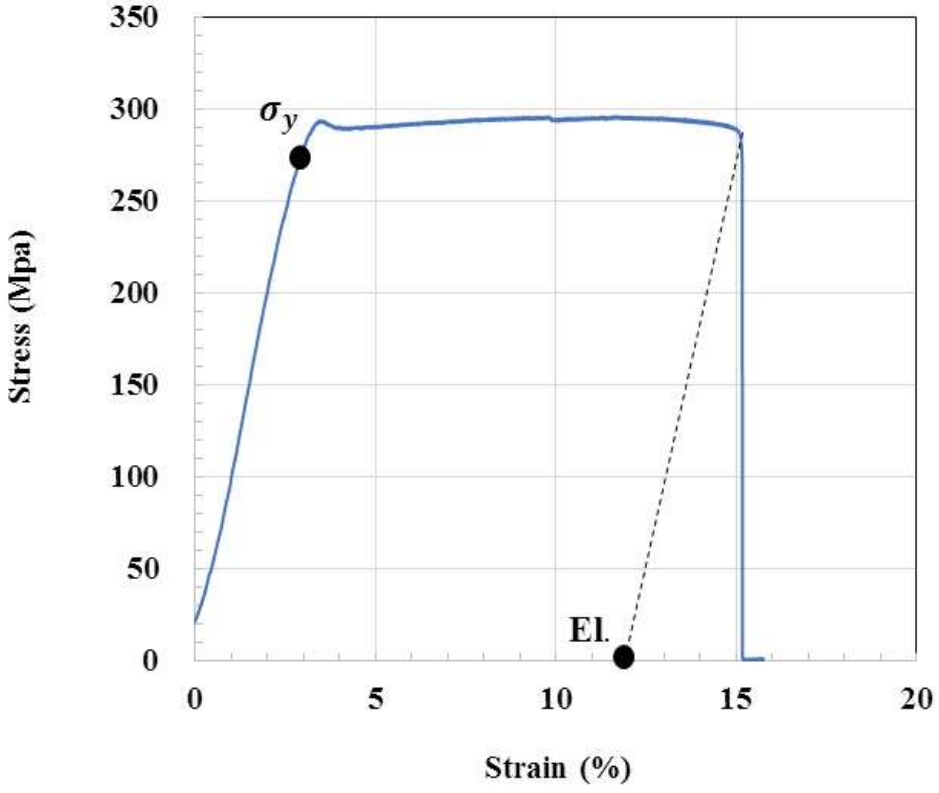
350
300
250
200
150
100
50
0
Stress (Mpa)
σ_y
El.
0
5
10
15
20
Strain (%)

Fig. 8